JCI insight

Mitochondrial CaMKII inhibition in airway epithelium protects against allergic asthma

Sara C. Sebag, … , Mark E. Anderson, Isabella M. Grumbach

JCI Insight. 2017;2(3):e88297. https://doi.org/10.1172/jci.insight.88297.

Research Article **Inflammation** **Pulmonology**

Excessive ROS promote allergic asthma, a condition characterized by airway inflammation, eosinophilic inflammation, and increased airway hyperreactivity (AHR). The mechanisms by which airway ROS are increased and the relationship between increased airway ROS and disease phenotypes are incompletely defined. Mitochondria are an important source of cellular ROS production, and our group discovered that Ca^{2+}/calmodulin-dependent protein kinase II (CaMKII) is present in mitochondria and activated by oxidation. Furthermore, mitochondrial-targeted antioxidant therapy reduced the severity of allergic asthma in a mouse model. Based on these findings, we developed a mouse model of CaMKII inhibition targeted to mitochondria in airway epithelium. We challenged these mice with OVA or *Aspergillus fumigatus*. Mitochondrial CaMKII inhibition abrogated AHR, inflammation, and eosinophilia following OVA and *A. fumigatus* challenge. Mitochondrial ROS were decreased after agonist stimulation in the presence of mitochondrial CaMKII inhibition. This correlated with blunted induction of NF-κB, the NLRP3 inflammasome, and eosinophilia in transgenic mice. These findings demonstrate a pivotal role for mitochondrial CaMKII in airway epithelium in mitochondrial ROS generation, eosinophilic inflammation, and AHR, providing insights into how mitochondrial ROS mediate features of allergic asthma.

JCI insight

RESEARCH ARTICLE

Mitochondrial CaMKII inhibition in airway epithelium protects against allergic asthma

Sara C. Sebag,[1] Olha M. Koval,[1,2] John D. Paschke,[1] Christopher J. Winters,[1] Omar A. Jaffer,[1] Ryszard Dworski,[3] Fayyaz S. Sutterwala,[1,2,4,5] Mark E. Anderson,[6,7] and Isabella M. Grumbach[1,2]

[1]Department of Internal Medicine, University of Iowa, Iowa City, Iowa, USA. [2]Veterans Affairs Healthcare System, Iowa City, Iowa, USA. [3]Division of Allergy, Pulmonary and Critical Care Medicine, Vanderbilt University, Nashville, Tennessee, USA. [4]Inflammation Program, University of Iowa, Iowa City, Iowa, USA. [5]Department of Medicine, Cedars-Sinai Medical Center, Los Angeles, California, USA. [6]Department of Medicine and [7]Department of Physiology, The Johns Hopkins University School of Medicine, Baltimore, Maryland, USA.

Excessive ROS promote allergic asthma, a condition characterized by airway inflammation, eosinophilic inflammation, and increased airway hyperreactivity (AHR). The mechanisms by which airway ROS are increased and the relationship between increased airway ROS and disease phenotypes are incompletely defined. Mitochondria are an important source of cellular ROS production, and our group discovered that Ca^{2+}/calmodulin-dependent protein kinase II (CaMKII) is present in mitochondria and activated by oxidation. Furthermore, mitochondrial-targeted antioxidant therapy reduced the severity of allergic asthma in a mouse model. Based on these findings, we developed a mouse model of CaMKII inhibition targeted to mitochondria in airway epithelium. We challenged these mice with OVA or *Aspergillus fumigatus*. Mitochondrial CaMKII inhibition abrogated AHR, inflammation, and eosinophilia following OVA and *A. fumigatus* challenge. Mitochondrial ROS were decreased after agonist stimulation in the presence of mitochondrial CaMKII inhibition. This correlated with blunted induction of NF-κB, the NLRP3 inflammasome, and eosinophilia in transgenic mice. These findings demonstrate a pivotal role for mitochondrial CaMKII in airway epithelium in mitochondrial ROS generation, eosinophilic inflammation, and AHR, providing insights into how mitochondrial ROS mediate features of allergic asthma.

Introduction

Asthma accounts for over 4,000 deaths annually and 2 million hospital visits (1). Existing treatments, such as bronchodilators and steroids, alleviate symptoms without selectively targeting specific pathologic mediators (2, 3). While numerous studies have provided evidence that asthma is a pleiotropic disease marked by increased airway ROS, the molecular mechanisms that connect ROS to asthma phenotypes are uncertain (4–7). We recently made the unanticipated discovery that the multifunctional Ca^{2+}/calmodulin-dependent protein kinase II (CaMKII) in airway epithelium is a key regulator of the ROS-linked asthmatic phenotypes of inflammation, eosinophilic recruitment and infiltration, and airway hyperreactivity (AHR) in murine models of allergic asthma (8).

Our group originally discovered that CaMKII is activated by ROS (ox-CaMKII) (9) and that ox-CaMKII is increased in airway epithelium from asthmatic patients after allergen exposure where it correlates with asthma severity (8). In subsequent studies, we found that mitochondrial-targeted antioxidant therapy protects against inflammation and fibrosis in OVA-challenged mice (10). These findings implicate both CaMKII and mitochondria in ROS-mediated pulmonary illnesses, including asthma. However, mechanistic insight is lacking.

In this study, we tested the hypothesis that, in response to allergen challenge, CaMKII in the mitochondria (Mt-CaMKII) of pulmonary airway epithelial cells contributes to an increase in mitochondrial ROS (Mt-ROS) and induction of hallmark features of allergic asthma. Utilizing a novel transgenic mouse model in which bronchial epithelial cells conditionally express a potent CaMKII inhibitor directed to mitochondria, we found that mitochondrial CaMKII inhibition significantly reduced *Aspergillus fumigatus*– and OVA-induced AHR, eosinophilic inflammation, and cytokine expression compared with WT controls. These hallmark

Conflict of interest: I.M. Grumbach and M.E. Anderson are named inventors on awarded patents related to CaMKII inhibition in asthma (US 8,440,656) and M.E. Anderson and O.M. Koval are named inventors on awarded patents related to targeting CaMKII inhibitors to mitochondria (US 9,168,307).

Submitted: April 29, 2016
Accepted: December 15, 2016
Published: February 9, 2017

Reference information:
JCI Insight. 2017;2(3):e88297.
doi:10.1172/jci.insight.88297.

features of allergic asthma were regulated in part by Mt-CaMKII–mediated, Mt-ROS–induced activation of NF-κB and the NLRP3 inflammasome. Taken together, our findings suggest that airway epithelial cell–derived Mt-CaMKII increases Mt-ROS that promotes induction of core features of allergic asthma. These data implicate Mt-CaMKII in multiple processes in the development of asthma. Mitochondrial-localized CaMKII inhibition may provide a new potential candidate target for future asthma therapies.

Results

Mitochondrial CaMKII inhibition reduces Mt-ROS generation and inflammation in airway epithelial cells. Mitochondrial dysfunction and excessive ROS generation are believed to promote allergic asthma (6, 7, 11–17). However, pathways specifically linking Mt-ROS to key mechanisms in allergic asthma have not been defined. In order to test the hypothesis that Mt-ROS and Mt-CaMKII contribute to allergic asthma, we first examined Mt-ROS levels from freshly isolated primary murine tracheal bronchial epithelial cells (MTBEC, ref. 18) taken from OVA-challenged mice, an established model of allergic airway disease (8). OVA exposure significantly increased Mt-ROS compared with saline control (Figure 1A). We identified CaMKII in the mitochondrial fraction of airway epithelium and tested whether ox-CaMKII was increased after OVA challenge (Figure 1B). Compared with saline controls, ox-CaMKII was significantly increased in both the cytosolic and mitochondrial fractions from lungs of allergen-challenged mice. Similarly, exposure of primary human airway epithelial cells (HAEC, ref. 19) to IL-13 increased ox-CaMKII in mitochondrial and cytoplasmic fractions (Figure 1C).

To test whether Mt-CaMKII activity in bronchial epithelial cells increases Mt-ROS and inflammation, we expressed a mitochondrial-targeted version (20) of the CaMKII inhibitor peptide, CaMKIIN (Mt-CaMKIIN, ref. 21), in cultured primary HAEC (Supplemental Figure 1, A and B; supplemental material available online with this article; https://doi.org/10.1172/jci.insight.88297DS1). CaMKIIN is the most potent CaMKII inhibitor peptide available and is notable for lacking activity against other calmodulin kinases or protein kinase C (21). Using two different methods, we established that Mt-CaMKIIN significantly blunted Mt-ROS production in response to cytokine agonist as compared with control (Figure 1, D and E). We next examined oxidative metabolism in HAEC after establishing the baseline oxygen consumption rate (OCR), which reflects the rate of electron transport in mitochondria (22). IL-13 induced an increase in OCR, suggesting enhanced oxidative metabolism, which has been shown to correspond with increased ROS (23), whereas expression of Mt-CaMKIIN blunted this effect (Supplemental Figure 1C).

With regards to proinflammatory mediator expression, IL-13 increased IL-5 mRNA levels (Figure 1, F and G), consistent with its established role as a Th2 cytokine that induces Mt-ROS and proinflammatory cytokines (10). In contrast, IL-13–mediated induction of IL-5 expression was abolished in Mt-CaMKIIN–expressing cells. These changes were not a result of enhanced viral-induced cell death, as analyzed by trypan blue exclusion assay (Supplemental Figure 1D). Analysis of mRNA expression of the epithelial-derived innate immune regulators thymic stromal lymphoprotein (TSLP, ref. 24, Figure 1H) and eotaxin (CCL11, ref. 25, Figure 1I) were found to be upregulated after exposure of HAEC to IL-13, while Mt-CaMKIIN–expressing cells showed reduced cytokine-mediated levels. Taken together, these data identify Mt-CaMKII in airway epithelial cells as a key mediator of the molecular response in allergic asthma.

Epithelial-targeted mitochondrial CaMKII inhibition reduces AHR after allergen challenge. To test the concept that Mt-CaMKII is important for allergic asthma in vivo, we generated mice with tamoxifen-inducible transgenic expression of HA-tagged CaMKIIN. Targeting of CaMKIIN to mitochondria in transgenic mice was achieved by fusion of the cox8a N-terminal domain to CaMKIIN (20). The strategy for generating mice with conditional expression of Mt-CaMKIIN (Cond-Mt-CaMKIIN) in CC10-positive airway epithelial cells is shown in Supplemental Figure 2A. In this model, EGFP is expressed in all tissues in Cond-Mt-CaMKIIN mice prior to tamoxifen-induced Cre recombination (Figure 2, A and B). Upon Cre recombination, EGFP cDNA is excised, allowing for controlled expression of the Mt-CaMKIIN transgene and concomitant loss of EGFP expression (Figure 2C). Robust transgene expression was detected only in mitochondrial fractions in Cond-Mt-CaMKIIN mice following Cre recombination (Figure 2D). As expected, Mt-CaMKIIN was not detected in the cytoplasmic fractions of any group (Figure 2D), confirming specific expression and delivery of Mt-CaMKIIN to mitochondria.

We next characterized the effect of Mt-CaMKIIN on allergen-induced ox-CaMKII mitochondrial expression from OVA-treated mice. WT animals treated with OVA had elevated ox-CaMKII expression compared with saline controls (Figure 2E). However, expression of Mt-CaMKIIN significantly

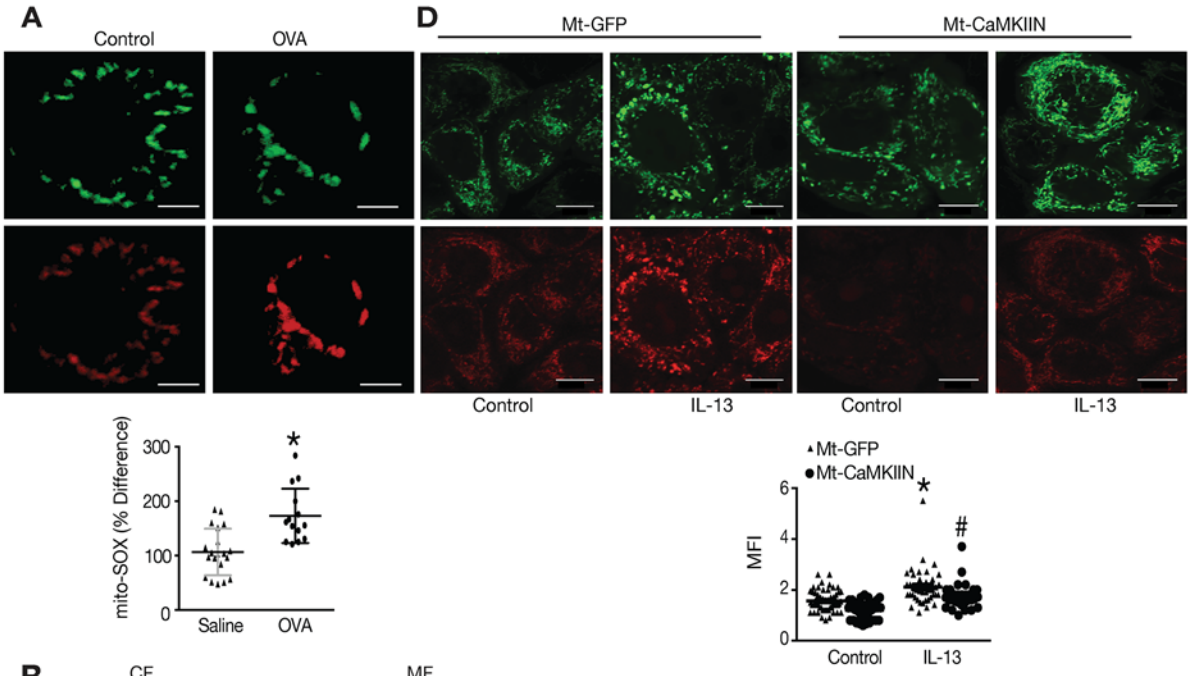
A
Control
OVA
D
Mt-GFP
Mt-CaMKIIN
Control
IL-13
Control
IL-13
mito-SOX (% Difference)
300
200
100
0
Saline
OVA
Mt-GFP
Mt-CaMKIIN
MFI
6
4
2
0
Control
IL-13

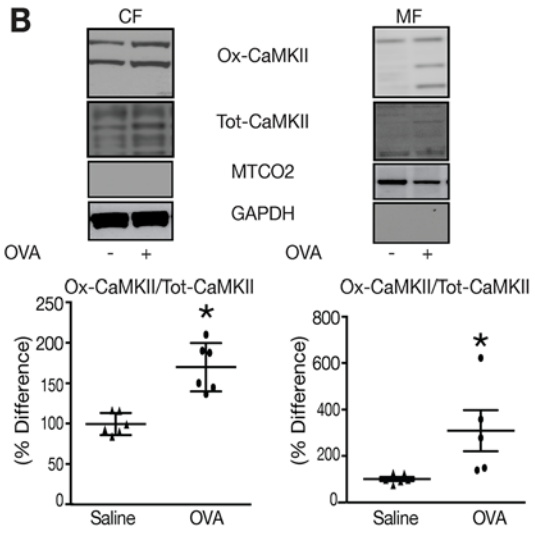
B
CF
MF
Ox-CaMKII
Tot-CaMKII
MTCO2
GAPDH
OVA
- +
OVA
- +
Ox-CaMKII/Tot-CaMKII
(% Difference)
250
200
150
100
50
0
Saline
OVA
Ox-CaMKII/Tot-CaMKII
(% Difference)
800
600
400
200
0
Saline
OVA

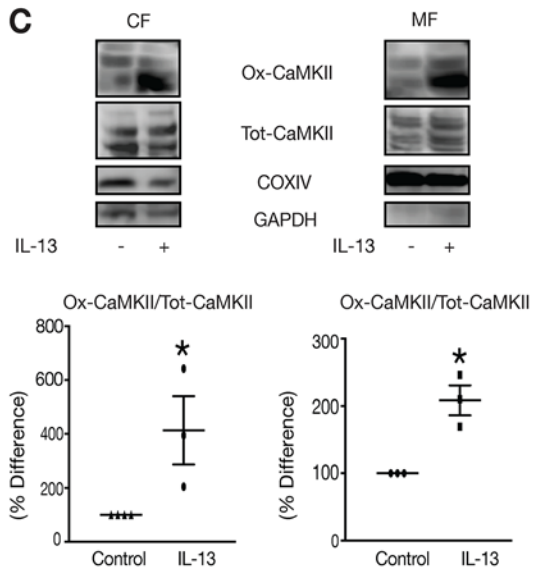
C
CF
MF
Ox-CaMKII
Tot-CaMKII
COXIV
GAPDH
IL-13
- +
IL-13
- +
Ox-CaMKII/Tot-CaMKII
(% Difference)
800
600
400
200
0
Control
IL-13
Ox-CaMKII/Tot-CaMKII
(% Difference)
300
200
100
0
Control
IL-13

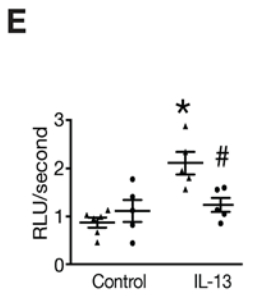
E
RLU/second
3
2
1
0
Control
IL-13

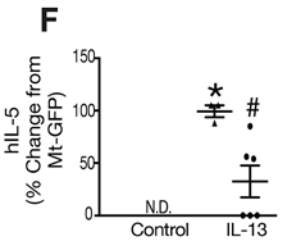
F
hIL-5
(% Change from Mt-GFP)
150
100
50
0
N.D.
Control
IL-13

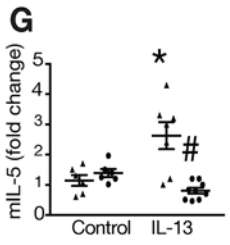
G
mIL-5 (fold change)
5
4
3
2
1
0
Control
IL-13

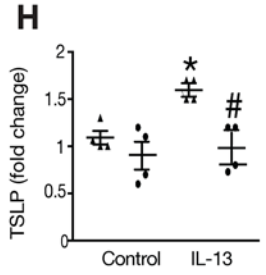
H
TSLP (fold change)
2
1.5
1
0.5
0
Control
IL-13

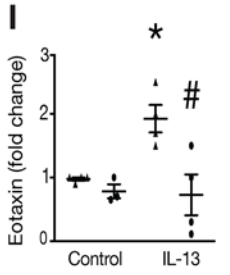
I
Eotaxin (fold change)
3
2
1
0
Control
IL-13

Figure 1. CaMKII in mitochondria of respiratory epithelial cells regulates mitochondrial ROS and IL-5 expression. (**A**) Representative images and quantification of mitochondrial ROS production in primary murine tracheal epithelial cells (MTBEC) isolated from WT mice after exposure to saline control (n = 6) or OVA (n = 15). Mitochondrial ROS production was determined with mitoSOX (red); MitoTracker (green) was used to colocalize mitochondria. Data were quantified for 10 images per treatment. Scale bar: 100 μm. (**B**) Immunoblots of active, oxidized, and total CaMKII in mitochondria from lungs of mice exposed to saline or OVA (n = 3–5). CF, cytoplasmic fraction; MF, mitochondrial fraction; MTCO2, mitochondrial protein marker; GAPDH, cytoplasmic protein marker. (**C**) Immunoblots of active oxidized and total CaMKII in mitochondria in mitochondrial and cytoplasmic fractions of primary human airway epithelial cells (HAEC) treated with media only (control) or IL-13 (10 ng/ml) for 48 hours (n = 3 independent experiments). COXIV, mitochondrial marker. (**D**) Representative images and quantification of mitochondrial ROS production in HAEC infected with Mt-GFP (empty) or Mt-CaMKIIN virus prior to exposure to IL-13 (10 ng/ml) for 2 days (n = 6 independent experiments; data were quantified for 10 images per treatment and represented as mean fluorescent intensity [MFI]). Scale bar: 100 μm. (**E**) ROS production by lucigenin assay in isolated mitochondria from HAEC treated as in **D** (n = 9 independent experiments). In **F–I**, triangles represent Mt-GFP, circles represent Mt-CaMKIIN. (**F** and **G**) IL-5 mRNA levels in HAEC or MTBEC (respectively) infected with Mt-GFP or Mt-CaMKIIN and treated as in **D**. Data in **F** are presented as the percentage change relative to Mt-GFP+IL-13 (n = 3 independent experiments). Data in **G** are presented as the fold change relative to Mt-GFP control (n = 3 independent experiments). (**H**) TSLP and (**I**) eotaxin mRNA levels in HAEC infected with Mt-GFP or Mt-CaMKIIN and treated as in **D** (n = 3–4 independent experiments). For **A–C** and **F**, Student's 2-tailed t test; for **D** and **E** and **G–I**, 1-way ANOVA with Tukey post-hoc test. $^{*}P < 0.05$ vs. control, $^{\#}P < 0.05$ vs. Mt-GFP+IL-13.

decreased OVA-mediated mitochondrial-localized ox-CaMKII (Figure 2E). Similar to previous findings (Figure 1A), WT mice had increased Mt-ROS in isolated MTBEC after OVA treatment (Figure 2F). In contrast, MTBEC from OVA-treated Mt-CaMKIIN mice showed reduced Mt-ROS (Figure 2F).

We next subjected WT and Mt-CaMKIIN mice to two different validated models of allergic asthma, *Aspergillus fumigatus* or OVA challenge (Supplemental Figure 2, B and C) (8). We measured airway resistance in response to increasing doses of methacholine. In WT mice, allergen challenge induced the expected increase in airway resistance as compared with saline-treated mice (Figure 2, G and H). However, Mt-CaMKIIN expression significantly reduced airway resistance after exposure to either allergen, demonstrating that mitochondrial CaMKII inhibition in airway epithelium reduces AHR in two established models of allergic asthma.

Mitochondrial-targeted CaMKII inhibition blunts allergen-induced eosinophil recruitment and infiltration. Accumulation of eosinophils in bronchoalveolar lavage fluid (BALF) is a hallmark of allergic asthma. Thus, we examined leukocyte recruitment to the lungs and BALF obtained from mice exposed to OVA and *A. fumigatus*. As expected, both *A. fumigatus* and OVA exposure increased recruitment of inflammatory cells to the BALF of WT mice (Figure 3, A and B). Mitochondrial CaMKII inhibition resulted in a reduction in total BALF cell counts compared with WT mice (Figure 3, A and B). This reduction corresponded with a significant decrease in the absolute numbers of BALF-derived eosinophils (Figure 3, C and D), whereas the numbers of total macrophages did not change between genotypes or treatment groups (Supplemental Figure 3, A and B). Histologic analysis of lung sections demonstrated that, following allergen challenge, eosinophil infiltration into the airway was significantly abrogated in Mt-CaMKIIN mice compared with WT mice (Figure 3, E and F, and Supplemental Figure 3C). In contrast to our earlier findings in mice with airway epithelial CaMKII inhibition without mitochondrial targeting (8), we did not detect appreciable differences in mucin staining between genotypes following allergen challenge (Figure 3, G and H). Thus, Mt-CaMKII plays a selective role in the recruitment and infiltration of eosinophils to the lung during allergic asthma without affecting mucus production.

Airway epithelial Mt-CaMKIIN inhibits NF-κB activation. We next investigated potential mechanisms by which Mt-CaMKII inhibition protected against key features of allergic asthma. The proinflammatory transcription factor, NF-κB, is a master regulator of inflammation in allergic asthma (26–30). We therefore asked if Mt-CaMKII inhibition reduces NF-κB activity and/or expression. A wide variety of agonists stimulate activation of NF-κB in lung epithelial cells that results in enhanced Th2 responses and eosinophilia. These include a component of Gram-negative bacteria, LPS (refs. 31, 32). Whereas challenge of HAEC with LPS (refs. 33, 34) resulted in pronounced translocation of the NF-κB p65 subunit to the nucleus and increased NF-κB transcriptional activity, expression of Mt-CaMKIIN significantly blunted NF-κB activation (Figure 4). In addition, other targets of NF-κB, including the inflammasome-associated protein NLRP3 (35) and the cytokine IL-1β (ref. 36), were also reduced in the presence of Mt-CaMKIIN (Supplemental Figure 4, A–C). These data show that mitochondrial CaMKII inhibition reduces a critical step in NF-κB activation and suggest reduced inflammatory responses to OVA and *A. fumigatus* could result from Mt-CaMKIIN suppression of NF-κB in airway epithelium.

Mitochondrial-targeted CaMKII inhibition attenuates expression of proinflammatory mediators. NF-κB–mediated expression of Th2 cytokines and chemokines drives recruitment and infiltration of eosinophils in allergic asthma (29, 37, 38). Club cells have recently been identified as the principal source of

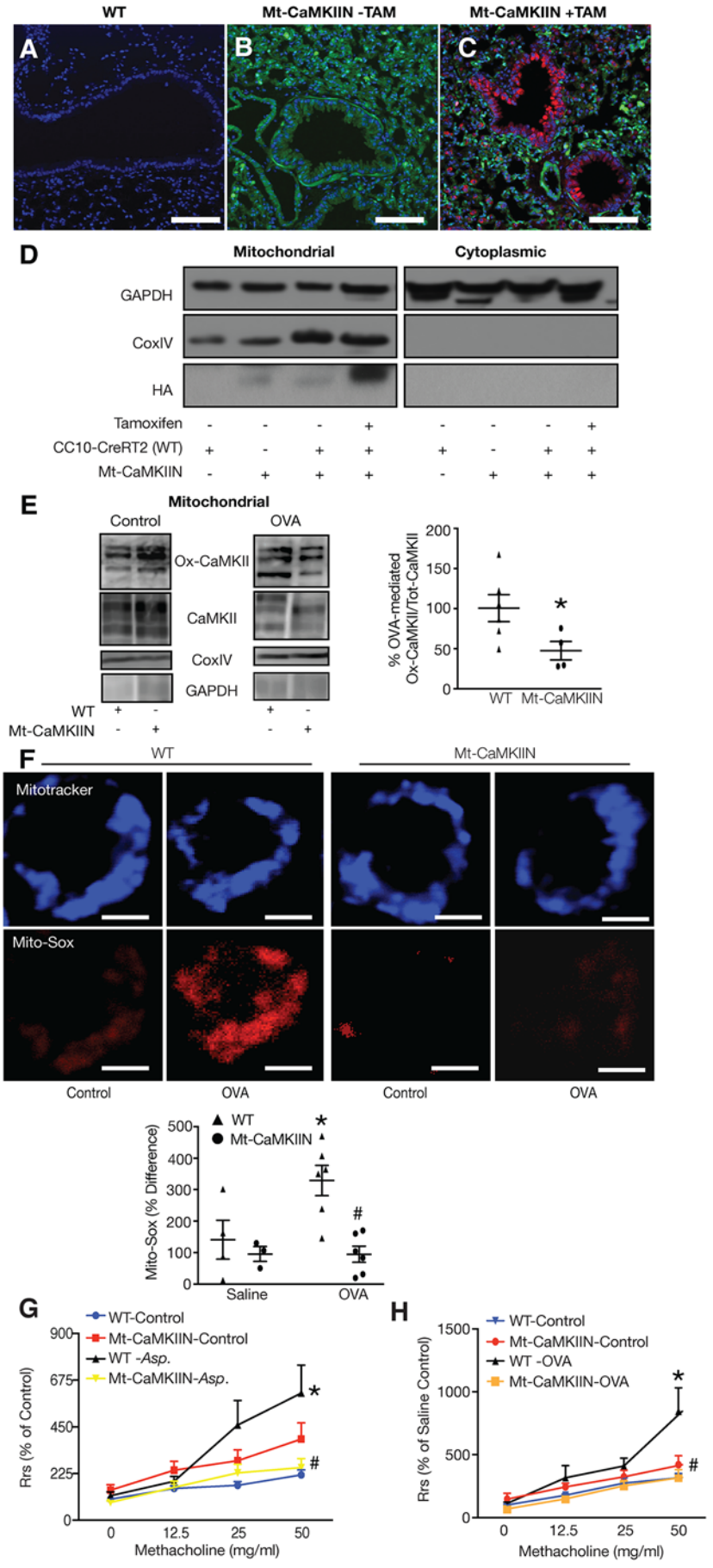

Figure 2. Mitochondrial CaMKII inhibition in respiratory epithelium attenuates airway hyperreactivity. (**A–C**) Immunofluorescence for GFP (green), HA-tagged Mt-CaMKIIN (red), and nuclei (TO-PRO-3, blue) in lung sections from (**A**) control CC10.CreRT2 mice (WT), (**B**) Mt-CaMKIIN mice without tamoxifen (TAM) treatment, or (**C**) Mt-CaMKIIN mice after tamoxifen treatment. Scale bar: 100 μm. (**D**) Immunoblots for HA-tagged Mt-CaMKIIN in mitochondrial and cytoplasmic fractions from lungs of WT and Mt-CaMKIIN mice without and with tamoxifen treatment. Lungs were harvested 10 days after the last administration of tamoxifen. (**E**) Immunoblots for ox-CaMKII in mitochondrial fractions from lungs of WT and Mt-CaMKIIN mice treated with OVA or saline control. Densitometric analysis of signal was normalized to COXIV control and then represented as percentage ox-CaMKII from WT-OVA (n = 4) versus Mt-CaMKIIN OVA (n = 3). Student's 2-tailed t test used. $^{*}P < 0.05$ vs. WT-OVA. (**F**) Representative images and quantification of mitochondrial ROS production in primary murine tracheal epithelial cells (MTBEC) isolated from WT or Mt-CaMKIIN mice after exposure to saline control (n = 3) or OVA (n = 6). Mitochondrial ROS production was determined with mitoSOX (red); MitoTracker (blue) was used to colocalize mitochondria. Data were quantified for 5–10 images per treatment. Scale bar: 100 μm. Two-way ANOVA with Tukey post-hoc test was used. $^{*}P < 0.05$ vs. control; $^{\#}P < 0.05$ vs. WT mice with OVA. (**G**) Airway hyperreactivity (AHR) in mice exposed to *A. fumigatus* (Asp) or control (Freund adjuvant alone) and challenged with increasing doses of methacholine (n = 6 WT control; 6 Mt-CaMKIIN control; 8 WT *A. fumigatus*; 8 Mt-CaMKIIN *A. fumigatus*–treated mice). (**H**) AHR in mice exposed to OVA or saline control and challenged with increasing doses of methacholine (n = 8 WT control; 9 Mt-CaMKIIN control; 10 WT OVA; and 12 Mt-CaMKIIN OVA–treated mice). Two-way ANOVA with Tukey post-hoc test was used. $^{*}P < 0.05$ vs. control; $^{\#}P < 0.05$ vs. WT mice with *A. fumigatus* or OVA exposure.

Th2-dependent eotaxin production in the lung (39, 40), as eotaxin is an eosinophil chemoattractant induced in different allergy models (25, 41) (Figure 1I). We found that Mt-CaMKIIN eliminated eotaxin mRNA expression following *A. fumigatus* or OVA challenge, in contrast to WT mice, in which eotaxin mRNA was significantly increased by *A. fumigatus* or OVA challenge (Figure 5, A and B). Eotaxin cooperates with other interleukins, including IL-4 and IL-5, to promote tissue eosinophilia (42, 43). Similar to eotaxin, induction of IL-4 and IL-5 in the lung by allergen challenge was attenuated by Mt-CaMKIIN expression (Figure 5, C–G). To assess the role of Mt-ROS in upregulating expression of IL-5 and IL-1β, mice were implanted with minipumps containing the control mitochondrial-targeted compound triphenyl phosphate or the Mt-ROS scavenger

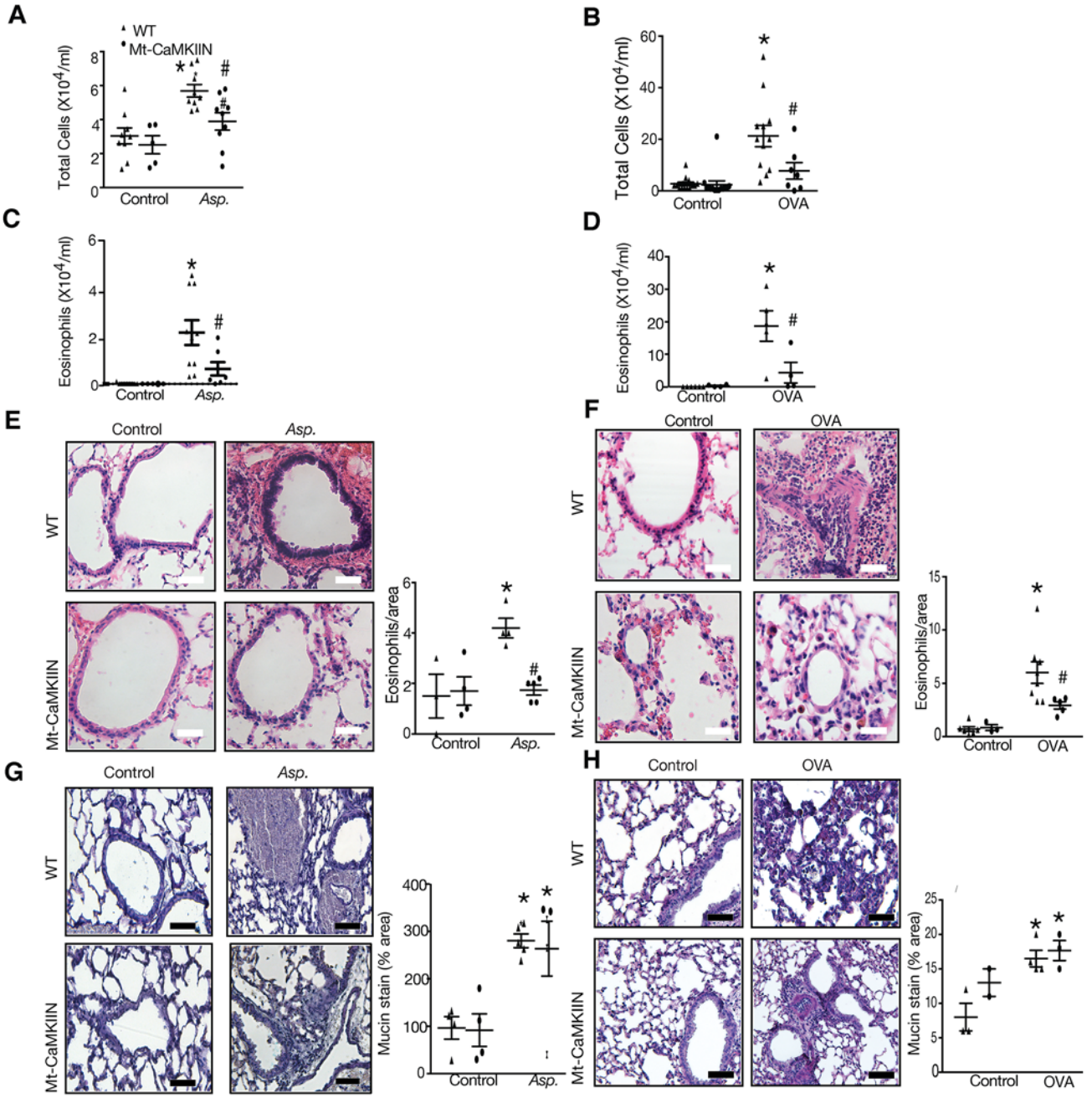

Figure 3. Allergen-induced eosinophilia is attenuated in Mt-CaMKIIN mice. (**A** and **B**) Total cell counts in bronchoalveolar lavage fluid (BALF) from mice exposed to (**A**) *A. fumigatus* or (**B**) OVA (*A. fumigatus*: $n = 7$ WT control; 5 Mt-CaMKIIN control; 10 WT *A. fumigatus*; and 8 Mt-CaMKIIN *A. fumigatus*–treated mice – OVA: $n = 14$ WT or Mt-CaMKIIN control; 13 WT OVA; and 7 Mt-CaMKIIN OVA-treated mice). Triangles: WT mice; circles: Mt-CaMKIIN mice. (**C** and **D**) Eosinophils in BALF from (**C**) *A. fumigatus*– or (**D**) OVA-exposed mice (*A. fumigatus*: $n = 7$ WT control; 5 Mt-CaMKIIN control; and 6–8 *A. fumigatus*–treated mice; OVA: $n = 6$–7 control; 5–6 OVA-treated mice). (**E** and **F**) Representative H&E staining and quantification of eosinophil infiltration in (**E**) *A. fumigatus*– and (**F**) OVA-challenged mice (original magnification, ×40, Scale bar: 50 μm). The number of eosinophils per 10 μm^2 area (original magnification, ×100, Scale bar: 1 mm) in 4–6 sections per mouse was quantified. (*A. fumigatus:* $n = 4$ WT control; 4 Mt-CaMKIIN control; and 4–5 *A. fumigatus*–treated mice; OVA: $n = 6$ WT control; 3 Mt-CaMKIIN control; 8 WT-OVA; and 5 Mt-CaMKIIN OVA-treated mice). (**G** and **H**) Representative PAS staining and quantification from (**G**) *A. fumigatus*– or (**H**) OVA-exposed mice (original magnification, ×20, scale bar: 25 μm). Data were quantified in 4–6 sections per mouse (*A. fumigatus*: $n = 4$ control and 5 *A. fumigatus*–treated mice; OVA: $n = 6$ control and 4–5 OVA-treated mice). $^*P < 0.05$ vs. control; $^\#P < 0.05$ vs WT mice with *A. fumigatus* or OVA exposure.

MitoTEMPO before OVA challenge. Similar to Mt-CaMKIIN mice, OVA-treated mice treated with MitoTEMPO had significantly ($P < 0.05$) reduced mRNA expression of both cytokines compared with control (Supplemental Figure 5, A and B). These data show that Mt-CaMKIIN mice reduce expression of allergen-mediated cytokines by reducing Mt-ROS production. Finally, assessment of IL-13 in the

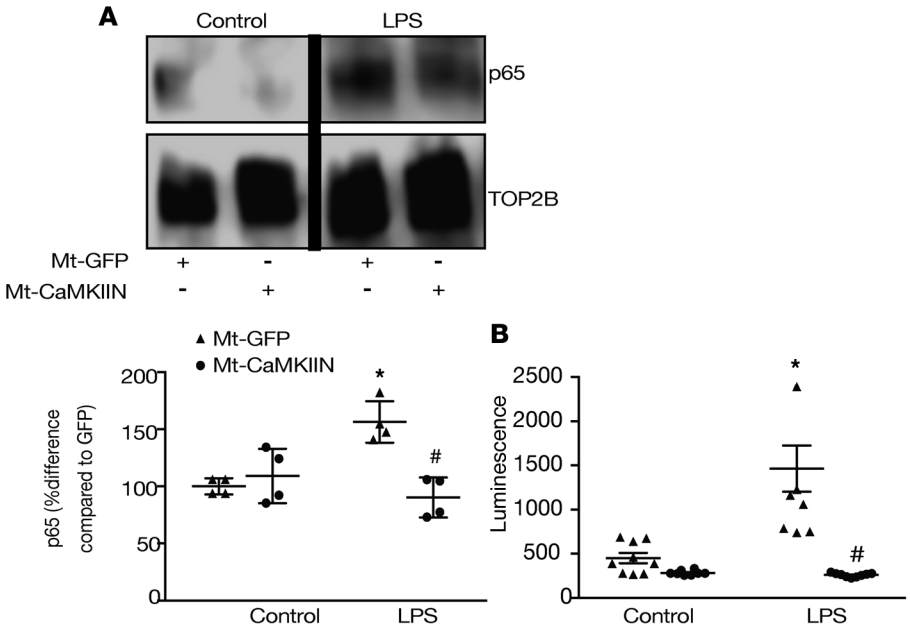

Figure 4. Epithelial cell Mt-CaMKIIN inhibition reduces LPS-mediated NF-κB activation. (**A**) Representative immunoblot and quantitation of nuclear NF-κB subunit p65 in HAEC infected with adenovirus containing Mt-GFP or Mt-CaMKIIN (10 MOI) and then exposed to control (media) or LPS (5 μg/ml) for 30 minutes. Data were quantified as the percentage difference relative to Mt-GFP control (n = 3 independent experiments). TOP2B, topoisomerase 2β. (**B**) NF-κB luciferase reporter activity in HAEC coinfected with adenoviruses containing NF-κB luciferase reporter and Mt-GFP or Mt-CaMKIIN. Cells were then exposed to LPS (1 μg/ml) for 24 hours. Triangles: Mt-GFP; circles: Mt-CaMKIIN (n = 9 independent experiments). ANOVA was used with Tukey post-hoc test. $^*P < 0.05$ vs. control; $^\#P < 0.05$ vs. Mt-GFP+LPS.

lung by allergen challenge showed a reduction in mice with Mt-CaMKIIN expression (Figure 5, H and I). These data show that Mt-CaMKIIN expression in airway epithelium has broad antiinflammatory consequences and suggest a previously unidentified role for Mt-CaMKII in allergen-induced expression of Th2 cytokines and chemokines.

Epithelial Mt-CaMKIIN inhibits NLRP3 inflammasome expression. Emerging evidence suggests that inflammasomes play a key role in the inflammatory response in asthma (44) by regulating Th2 differentiation and expression of interleukins (35, 45, 46). In addition, Mt-ROS production has been linked to NLRP3 inflammasome expression and activity (16, 35, 47–50). We found that while LPS challenge induced mRNA and protein expression of NLRP3 (Figure 6A and Supplemental Figure 4A), active caspase-1 (p20), and the mature, bioactive form of IL-18 in HAEC, Mt-CaMKIIN decreased expression and activation of these inflammasome-associated proteins (Figure 6A and Supplemental Figure 4A). We next examined NLRP3 inflammasome activation in vivo. OVA in the presence of alum has been shown to induce NLRP3 expression (51). Challenge with either OVA (in the presence of alum) or *A. fumigatus* induced expression of NLRP3 inflammasome proteins in the lungs of WT mice, but this response was significantly reduced in Mt-CaMKIIN mice following allergen challenge (Figure 6, B and C). To address whether NLRP3 activation is directly dependent on expression of Mt-CaMKII in airway epithelial cells, HAEC were infected with an adenovirus expressing Mt-CaMKII. Overexpression of Mt-CaMKII was sufficient to increase levels of mature IL-18 (Figure 6D), whereas treatment of cells with the NLRP3 inhibitor MCC950 (52) abolished Mt-CaMKII–mediated effects. These data provide evidence that Mt-CaMKII inhibition ablates NLRP3 inflammasome activity in allergic asthma.

Increased NLRP3 and IL-18 expression in airway epithelium from atopic asthmatic patients. Our data provide evidence for a pathway in airway epithelium where allergens increase inflammatory signaling by activating NF-κB and inflammasomes. While NF-κB signaling is firmly established to promote asthma in patients, the role of inflammasome signaling is less established. In order to test for the translational relevance of our findings related to inflammasome activation, Mt-CaMKII and Mt-ROS in experimental models, we next determined NLRP3 and IL-18 protein expression in lungs from nonasthmatic and from atopic asthmatic patients (Supplemental Table 1). We found that expression of NLRP3 and IL-18 was increased significantly in lung biopsies from asthmatic patients, specifically in the airway epithelium, compared with healthy controls (Figure 7). These data suggest that increased NLRP3 inflammasome expression in airway epithelium is increased in asthma.

Discussion

Asthma is a condition of increased ROS, airway inflammation, and AHR (5, 37, 40, 53). Airway epithelial ox-CaMKII is increased in asthmatic patients and transduces elevated ROS to promote allergic asthma in mouse models (8). Mitochondrial dysfunction and Mt-ROS are emerging concepts

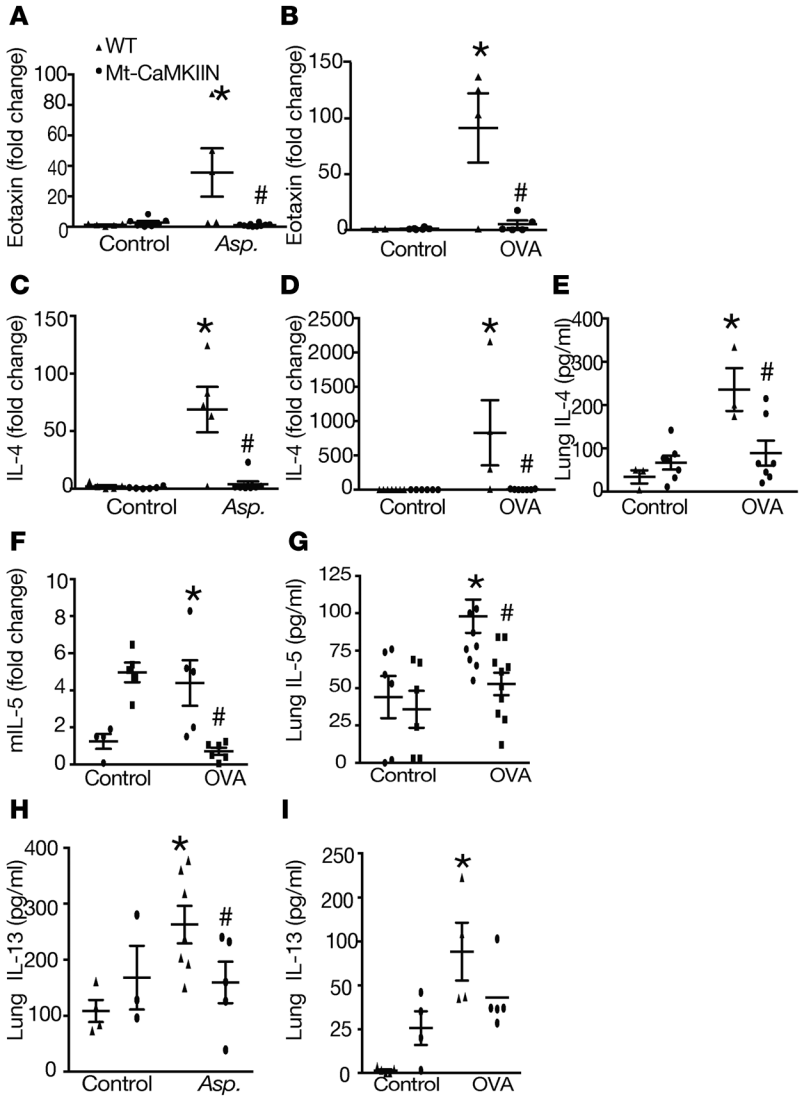

Figure 5. Mt-CaMKII inhibition in airway epithelium abrogates allergen-induced inflammatory cytokine expression in vivo. (**A** and **B**) qRT-PCR for eotaxin in lungs from (**A**) *A. fumigatus*– or (**B**) OVA-challenged WT or Mt-CaMKIIN mice (n = 5–7 controls and 5 WT *A. fumigatus* and 10 Mt-CaMKIIN *A. fumigatus*–treated mice or 3 controls and 4–5 OVA-treated mice). (**C** and **D**) qRT-PCR for IL-4 in lungs of (**C**) *A. fumigatus*– or (**D**) OVA-challenged WT or Mt-CaMKIIN mice (n = 5–6 controls and 5 WT *A. fumigatus* and 9 Mt-CaMKIIN *A. fumigatus*–treated mice or 7–8 controls and 9–10 OVA-treated mice). (**E**) ELISA for IL-4 protein in lungs from OVA-challenged WT or Mt-CaMKIIN mice (n = 3 WT control; 8 Mt-CaMKIIN control; 4 WT-OVA; and 7 Mt-CaMKIIN OVA-treated mice). (**F**) qRT-PCR for IL-5 in lungs from OVA-challenged WT or Mt-CaMKIIN mice (n = 7–8 controls and 9–10 OVA-treated mice). (**G**) ELISA for IL-5 in lungs from mice after OVA challenge (n = 6 controls and 10 OVA-treated mice). (**H** and **I**) ELISA for IL-13 protein in lungs of (**H**) *A. fumigatus*– or (**I**) OVA-challenged WT or Mt-CaMKIIN mice (n = 4 controls and 8 *A. fumigatus*–treated mice or 4–5 controls and 5–7 OVA-treated mice). ANOVA was used with Tukey post-hoc test. $^{*}P < 0.05$ vs. control or saline; $^{\#}P < 0.05$ vs. WT mice with *A. fumigatus* or OVA exposure. Triangles: WT mice; circles: Mt-CaMKIIN mice.

in asthma; however, sources of these phenomena are unclear (6, 7, 10–12, 54). One potential clue is that mitochondrial CaMKII inhibition is protective in a variety of myocardial injury models linked to elevated ROS and mitochondrial dysfunction (7, 20, 55, 56). Here, we show increased levels of ox-CaMKII in the mitochondria of murine lung homogenates and primary HAEC after allergen challenge, while inhibition of Mt-CaMKII reduced expression and Mt-ROS production. Inhibition of mitochondrial CaMKII protects against OVA- and *A. fumigatus*–induced allergic lung disease, including reduction of NLRP3 inflammasomes, Th2 cytokines, eosinophilic inflammation, and AHR (Figure 8). Our data position Mt-CaMKII in airway epithelium as a key regulator of Mt-ROS in allergic asthma.

Taken together with our earlier model of extramitochondrial CaMKII inhibition in airway epithelium (8), our data suggest subcellular specificity to CaMKII signaling in allergic asthma (57). Untargeted CaMKII inhibition reduces allergen-induced mucus production via a mechanism that includes regulation of chloride current (I_{Cl}) through γ-aminobutyric acid type A receptor (GABAAR) (7). GABAAR is expressed on the apical surface of bronchial epithelia (58, 59). The fact that mucus production was not altered in our model strengthens our conclusion that CaMKII was specifically inhibited in the mitochondria without modifying CaMKII-mediated effects in the cytosol and suggests there are multiple signaling pathways regulated by CaMKII in distinct cellular compartments (57). We also studied changes in lung-derived IL-13, a known inducer of mucus production and secretion (60). Our data showed that IL-13 was increased in both *A. fumigatus*– and OVA-treated WT mice, while inhibition of Mt-CaMKII reduced expression. However, other models of allergic asthma demonstrate mucus secretion and expression through IL-13–independent pathways, including the cytokines IL-17A and IL-6 (61, 62). This suggests that, in addition to subcellular-specific effects, lung epithelial-derived Mt-CaMKII does not target IL-6 or Th17 signaling pathways (63), while many of the other core phenotypes of allergic asthma, including Th2 mediator production, eosinophilic inflammation, and AHR, are blunted.

NF-κB is a redox-sensitive transcription factor (64), and mitochondrial oxidative stress has been linked to NF-κB activation, leading to increased inflammation (65, 66). CaMKII modulates various proinflamma-

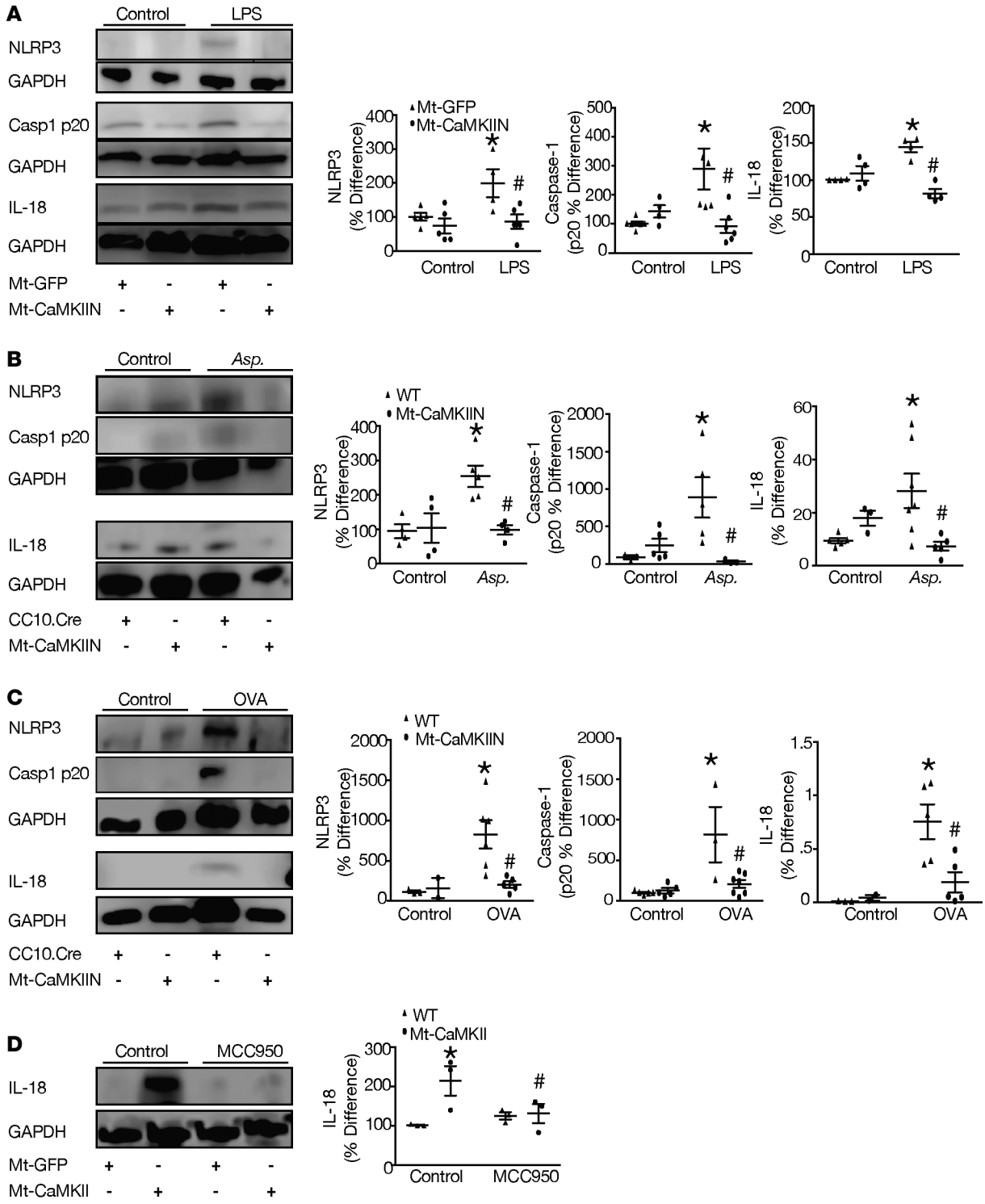

Figure 6. Epithelial Mt-CaMKII inhibition reduces expression of inflammasome proteins. (**A**) Immunoblots and quantitation for inflammasome proteins NLRP3, active caspase-1 (p20), and bioactive IL-18 in HAEC were infected with adenovirus containing Mt-GFP or Mt-CaMKIIN and treated with control or LPS (5 μg/ml) for 24 hours. GAPDH, loading control (n = 4–5 independent experiments). Triangles: WT mice; circles: Mt-CaMKIIN mice. (**B**) Immunoblots and quantitation for inflammasome proteins in lung homogenates from WT or Mt-CaMKIIN mice challenged with *A. fumigatus* (n = 3–5 mice/group). (**C**) Immunoblots and quantitation for inflammasome proteins in lung homogenates from WT or Mt-CaMKIIN mice challenged with OVA (n = 3–5 mice/group). (**D**) Immunoblot and quantification of bioactive IL-18 in HAEC infected with adenovirus containing Mt-GFP or Mt-CaMKII and treated with control (DMSO, 0.1%) or MCC950 (7.4 nM) for 24 hours. GAPDH, loading control (n = 3 independent experiments). Data were quantified as the percentage difference from Mt-GFP control (**A** and **D**) or WT control (**B** and **C**). ANOVA with Tukey post-hoc test. $^{*}P < 0.05$ vs. control; $^{\#}P < 0.05$ vs. Mt-GFP control or WT mice with *A. fumigatus* or OVA exposure.

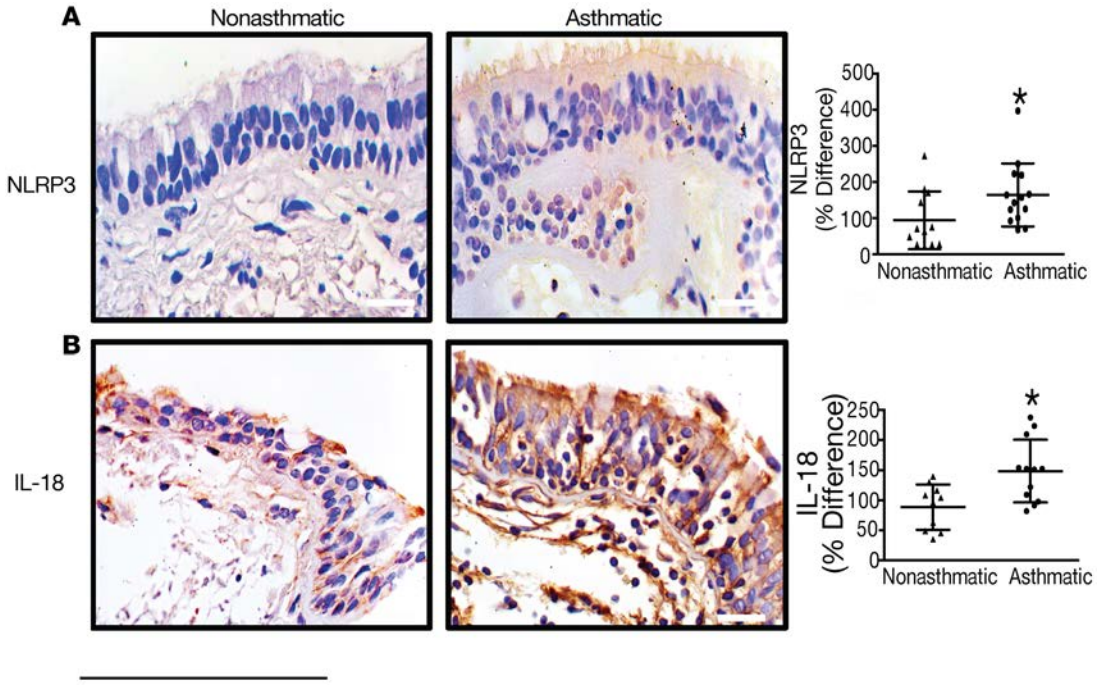

Figure 7. NLRP3 and IL-18 are increased in the airway epithelium of patients with established asthma. Representative staining and quantification of NLRP3 (**A**) and IL-18 (**B**) from lung sections of nonasthmatics (n = 6) or patients with atopic asthma (n = 9). Data were quantified as the percentage difference relative to nonasthmatic samples. Scale bar: 50 μm. Student's 2-tailed t test was used. *$P < 0.05$ vs. nonasthmatic.

tory signaling pathways, particularly those linked to NF-κB (8, 67, 68). Previous studies utilizing intranasal instillation of KN-93, a pharmacological inhibitor of CaMKII, demonstrate reduction of NF-κB activity in OVA-challenged mice (8). In acute asthma, mitochondria generate superoxide that is converted to hydrogen peroxide. This compound can then reach the cytoplasm after opening of the mitochondrial transition pore (refs. 69–71); thereby, hydrogen peroxide generated in mitochondria acts as a signaling mediator that induces NF-κB activation (12, 72). Our data are in support of these studies, as we found that epithelial Mt-CaMKIIN expression reduced stimulant-mediated oxidative stress and altered mitochondrial function (measured by Mt-ROS and OCR), which correlated with reduced NF-κB activation. Although drugs that target NF-κB are currently in development (73), there is concern that long-term NF-κB inhibition may result in immune suppression and impairment of host defenses (2). As such, mitochondria-targeted CaMKII inhibition (which did not cause increased toxicity of airway epithelial cells compared with control virus) may prevent excessive, pathological NF-κB activation without negative consequences of "direct" NF-κB inhibition.

Both NF-κB activation and Mt-ROS generation have been implicated in the activation of NLRP3 inflammasomes (16, 35, 47, 65, 74, 75), with emerging data suggesting a role for inflammasomes in a variety of lung diseases (16, 31, 44–46, 76–78). In a model of house dust

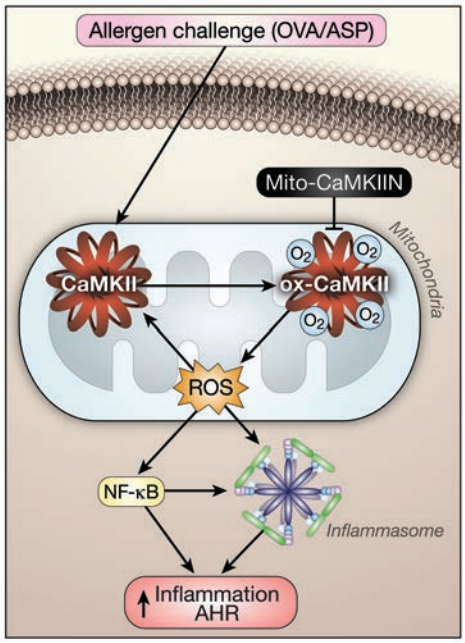

Figure 8. Schematic representation of findings. Exposure of lung epithelial cells to an allergic stimulus induces ox-CaMKII expression in mitochondria, leading to Mt-ROS generation. This in turn activates NF-κB, which, together with inflammasome expression and activation, induces the expression of Th2 cytokines, including eotaxin, IL-4, and IL-5, leading to eosinophil recruitment and infiltration as well as increased airway hyperreactivity.

mite–induced asthma, airway epithelial NLRP3 expression correlates with enhanced asthma phenotypes, which can be reduced by scavenging Mt-ROS (16). Activation of NLRP3 in dendritic cells by bacterial challenge identified a role for NLRP3/caspase-1/IL-18 in promoting allergic asthma (78). In addition, in diet-induced obesity, NLRP3 induces innate lymphoid cell–mediated AHR (79). Relevant to our study, the NLRP3 pathway has also been implicated in OVA-induced asthma (51), and we extend these findings by demonstrating NLRP3 activation in the *A. fumigatus* model. Importantly, we found that targeted inhibition of CaMKII in mitochondria of airway epithelial cells reduced NLRP3 expression, caspase-1 activation, and mature IL-18. Additionally, overexpression of Mt-CaMKII in HAEC led to the induction of mature IL-18, which was ablated in the presence of an NLRP3 inhibitor. Finally, we found in human lung sections that, compared with normal individuals, atopic asthmatics have significantly increased NLRP3 and IL-18 expression in airway epithelium. Taken together, these data in mouse models demonstrate that Mt-CaMKII exerts proinflammatory effects through multiple pathways, including NF-κB and NLRP3 inflammasome activation that converge on downstream induction of Th2 cytokines. The finding of increased inflammasome expression in patients suggests these pathways, defined in mice, may be relevant to humans.

In summary, our study provides evidence suggesting that excessive CaMKII activity in mitochondria of airway epithelium drives a cascade of Mt-ROS–dependent events, leading to key asthma phenotypes. Further studies will be required to determine which targets are critical for CaMKII to induce Mt-ROS as well as if activation of Mt-CaMKIIN after establishment of asthma is therapeutically relevant. Regardless, the translational potential of our findings is high, given that CaMKII inhibitors and mitochondrial targeting strategies that improve mitochondrial accumulation and retention of therapeutic agents are currently under development (53, 80). Targeting CaMKII in airway epithelia could be achieved with an inhaled agent, thus limiting potential side effects associated with CaMKII inhibition in other cell types. Moreover, the apparent link between Mt-CaMKII, Mt-ROS, NF-κB, and NLRP3 inflammasome activation in OVA- and *A. fumigatus*–challenged mice could have implications for other diseases marked by elevated ROS and inflammation.

Methods

Generation of mice and strains. Mice with tamoxifen-inducible Cre recombinase driven by the CC10 promoter (81) on a C57BL/6 background (denoted as "CC10-CreRT2 mice or CC10-Cre mice") were obtained from Jackson Laboratories. HA-tagged Mt-CaMKIIN mice were generated by cloning cDNA for the HA-tagged CaMKII inhibitor peptide CaMKIIN (HA-CaMKIIN) (20, 82) fused with the mitochondria targeting Cox8-palmitoylation sequence (20) into a construct containing the CX-1 promoter and a floxed enhanced GFP sequence (83), also on a C57BL/6 background. Double-transgenic mice, denoted as "Mt-CaMKIIN mice," were generated by crossing CC10-CreRT2 mice with HA-tagged Mt-CaMKIIN mice, as diagrammed in Supplemental Figure 2A. All mice were genotyped by established methods.

Club cell–specific expression of the peptide CaMKIIN was induced in 6- to 8-week-old male and female (equal proportions) mice via i.p. injection of tamoxifen dissolved in corn oil (5 days, 0.25 mg/g, Supplemental Figure 2). HA transgene expression was verified by immunofluorescence using GFP and anti-HA antibody in 10-μm frozen lung sections (HA Epitope Tag Antibody [16B12], 1:200, catalog A-21288, ThermoFisher Scientific). Sections were imaged using a LSM 510 confocal microscope (Carl Zeiss). Low levels of expression of HA-tagged CaMKIIN (leak) were detected in mitochondria from both the HA-tagged Mt-CaMKIIN mice (lacking the CC10.Cre transgene) and in double-transgenic Mt-CaMKIIN mice in the absence of tamoxifen-induced Cre recombination (see Figure 2D). In order to reduce any confounding effects due to Mt-CaMKIIN leak, all studies used tamoxifen-treated CC10-CreRT2 mice as WT littermate controls.

Murine models of allergic asthma. Beginning 10 days after the first tamoxifen injection (day 0), allergic asthma was modeled in vivo by challenge with *A. fumigatus* or OVA, as shown in Supplemental Figure 2, B and C, and as previously described (8). For the *A. fumigatus* model, mice were sensitized on day 0 via single i.p. and s.c. injections with a total of 20 μg of *A. fumigatus* crude extract (catalog XPM3D3A25, Greer Laboratories) dissolved in 0.2 ml of incomplete Freund adjuvant (catalog F5881, Sigma-Aldrich). Next, mice were challenged with 4 intranasal instillations of 10 μg of *A. fumigatus* on days 7, 14, 21, 28, and 32. An equal volume of Freund adjuvant was administered to control mice. For the OVA model, mice were sensitized by i.p. injection of 10 μg of OVA (catalog A7641, Sigma-Aldrich) mixed with 1 mg of alum (or saline alone, for control mice) on days 0 and 7. Mice were subsequently challenged with inhaled OVA (catalog A5503, Sigma-Aldrich, 1% solution in 0.9% saline, 40-minute challenge) or saline on days 14–17 (Supplemental Figure 2).

Epithelial cell culture and Mt-CaMKIIN adenoviral expression. Primary murine tracheal epithelial cells were isolated from B62 mice (obtained from Charles River Laboratories) as previously described (18). For expression of Th2 cytokines, cells were plated onto collagen–coated (BD Biosciences) coverslips and maintained in MTEC Plus culture medium as described previously (18). Cells were grown until confluent and then infected with either adenovirus containing the cDNA for mitochondrial-targeted GFP (Mt-GFP, empty vector) or Mt-CaMKIIN (both at 10 MOI) for 6 hours. Adenoviral vectors were generated by the University of Iowa Gene Vector Core Facility. In some experiments, cells were challenged with recombinant murine IL-13 (10 ng/ml, catalog 413-ML-005/CF, R&D Systems) for 14 days.

Primary HAEC were obtained from the Cells and Tissue Core, University of Iowa, Division of Pulmonary Medicine (19). Cells were grown in keratinocyte serum-free media (Gibco) and routinely tested for mycoplasma contamination. Early passages were treated with adenovirus-expressing Mt-CaMKIIN or empty vector control virus (Mt-GFP) for 48 hours (both at 10 MOI). In some experiments, cells were incubated with recombinant human IL-13 (10 ng/ml, catalog 213-ILB/CF) for 48 hours or 5 μg/ml LPS (*Escherichia coli* 055:B5, catalog L2880, Sigma-Aldrich) for 30 minutes (for NF-κB experiments) or 24 hours (for NLRP3 inflammasome expression analysis; for mRNA levels in Supplemental Figure 4). For NLRP3 inhibition, cells were infected with Mt-GFP or Mt-CaMKII (10 MOI). After 48 hours, cells were exposed to MCC950 (7.4 nM, catalog 17510, Cayman Chemical, ref. 52) for 24 hours. For NF-κB p65 immunoblots, nuclear fractions were isolated using the NE-PER nuclear and cytoplasmic extraction kit (catalog 78833, Thermo Scientific).

Assessment of AHR. AHR in response to methacholine was measured after the last *A. fumigatus* or OVA exposure on a flexiVent small-animal ventilator (Scireq) using a single compartment model, giving the dynamic resistance of the respiratory system (R), as described previously (8).

Bronchoalveolar lavage and cell differential. After the assessment of AHR, mice were euthanized. The trachea was cannulated, and two phosphate-buffered saline washings were collected for total and differential counts of lavage cells. BALF cellular differential was determined on 250 μl cytospins stained with Diff-Quik (Dade Behring).

Murine lung histology. Lungs were fixed with 4% paraformaldehyde and then processed by paraffin embedding. Tissue sections (5 μm) were stained using H&E or Alcian Blue/PAS to determine mucin distribution. Images were taken on an Olympus BX-61 light microscope (Olympus). Eosinophilia from H&E sections was determined using the ×100 objective; 4–7 random digital images per group were taken within areas of overt peribronchiolar inflammation. Total eosinophil cell counts were determined using NIH ImageJ software (ImageJ64, version 1.48, NIH) and expressed as number of cells per 10-μm area. For mucin measurements, PAS-stained slides were imaged (×20 objective), and then ImageJ software was used to determine the percentage of positive stained area per total area.

Cytokine analysis by ELISA. Homogenates of flash-frozen lungs were prepared in radioimmunoprecipitation assay (RIPA) buffer with phosphatase and protease inhibitors. IL-4, IL-5, and IL-13 were analyzed in lung homogenates by cytokine-specific ELISA Duo Set kits (catalog DY404, DY405, and DY413, respectively, R&D Systems).

Quantitative real-time PCR. Total RNA was isolated using the Qiagen RNeasy column-based kit. Complementary DNA was prepared using the SuperScript III reverse transcription system (Invitrogen) with random nanomer primers. Expression of mRNA was quantified with the iQ LightCycler (Bio-Rad) and SYBR Green dye system and normalized to acidic ribosomal phosphoprotein 1 (Arp) mRNA for mouse mRNA or GAPDH for human RNA analysis. Primer sequences are provided in Supplemental Material.

Mitochondria isolation. Freshly collected HAEC or murine lung homogenates were suspended in ice-cold mannitol, sucrose, EGTA (MSE) buffer [5 mM 3-(N-morpholino) propanesulfonic acid, 70 mM sucrose, 2 mM ethyleneglycol-bis-(b-aminoethyl ether)-N, N9-tetraacetic acid, 220 mM mannitol, pH 7.2, with KOH] and then homogenized. Nuclei and unbroken cells were pelleted by centrifugation twice at 600 *g* for 5 minutes. The crude mitochondrial and cytosolic fraction was obtained from the supernatant by centrifugation at 8,500 *g* for 10 minutes. The pellet was then resuspended in 100 μl MSE with protease and phosphatase inhibitors. Finally, samples were centrifuged at 8,500 *g* for 10 minutes, and the pellet was resuspended in 50 μl MSE with protease and phosphatase inhibitors.

Mt-ROS detection with mitoSOX. ROS were measured in live-cultured HAEC or freshly isolated murine cells using the dihydroethidium derivative mitoSOX red (5 mM, catalog D1168, Invitrogen). The mitochondrial localization of staining was confirmed by colocalizing with MitoTracker green or deep red (50 nM, catalog M7514 or catalog M22426, respectively, Thermo Fisher Scientific). Cells were imaged using a

LSM 510 confocal microscope (Carl Zeiss) and analyzed with NIH ImageJ. All images were taken at the same time and using the same imaging settings. Data are presented as percentage difference from controls.

Lucigenin assay. The rate of superoxide anion formation was determined in isolated mitochondria by lucigenin (bis-N-methylacridinium nitrate, catalog M8010, Sigma-Aldrich) as described previously (10, 84). Briefly, 100 μl of substrate nicotinamide adenine dinucleotide phosphate reduced (100 μM) was added to 20 μg of mitochondrial protein lucigenin (5 μM). Chemiluminescence was monitored every 15 seconds for 10 minutes, and the rate of change was expressed as relative light units per second.

Immunoblots. Homogenates of flash-frozen lungs or cell lysates were prepared in RIPA buffer with phosphatase and protease inhibitors. The proteins were separated by SDS-PAGE and transferred to a PVDF membrane. The membrane was then incubated with primary antibodies against pan-CaMKII (1:250, catalog 07-1496, Millipore); ox-CaMKII (1:250, immune sera, ref. 20), human p65 (1:500, catalog sc-109, Santa Cruz), human topoisomerase IIβ (1:500, catalog sc-13059, Santa Cruz), NLRP3 (1:500 catalog AG-20B-0014, Adipogen), Caspase-1 (p20, 1:500, catalog sc-1218, Santa Cruz), human IL-18 (1:1,000, catalog 04-1503**,** Millipore), mouse/human IL-18 (1:500, catalog sc-7954, Santa Cruz), GAPDH (1:2,000, catalog 2118S, Cell Signaling), COXIV (1:2,000, catalog 4850, Cell Signaling), or MTCO2 (1:500, catalog ab3298, Abcam) followed by incubation with the appropriate HRP-conjugated anti-goat (1:1,000; catalog HAF017, R&D Systems), anti-mouse (1:1,000, catalog 7076, Cell Signaling), or anti-rabbit (1:1,000, catalog sc-2004, Bio-Rad) IgG secondary antibody.

Human subjects. Nonsmoking asthmatics volunteers with a physician diagnosis of mild atopic asthmatic according to National Asthma Education and Prevention Program (85) were recruited from Vanderbilt University. All participants had a positive skin test with aeroallergens typical for this area, methacholine test, and inhaled allergen challenge. Asthma drugs were stopped for at least 48 hours prior to experimental procedures. Two patients used intermittently inhaled corticosteroids for seasonal asthma exacerbation but not during the period of the study. All women had negative urine HCG tests.

Experimental procedures. Prick skin test was done with diluent and histamine controls and a set of standardized allergens (*Dermatophagoides pteronyssinus, Dermatophagoides farina,* catalog hair, Bermuda grass, Kentucky bluegrass, fescue meadow grass, orchard grass, redtop grass, rye grass, sweet vernal grass, timothy grass, and short ragweed, Greer Labs) (86). The methacholine (Methapharm Inc.) challenge was performed using a Salter dosimeter (Salter Labs) and Flow Screen spirometer (VIASYS Healthcare GmbH) (87). Provocations with inhaled allergen were carried out using the protocol described by Cockcroft and colleagues (88). Allergen aerosols were generated using a Wright nebulizer connected to a 2-way Hans Rudolph valve mouthpiece (Roxon) attached to a wall oxygen source at 50 psi. Fiberoptic bronchoscopy with 4 endobronchial biopsies was performed in the lingua of the left upper lobe. Patients fasted overnight before bronchoscopy. Intravenous midazolam (1–2 mg) and fentanyl (50–100 mcg) were administered for sedation and topical lidocaine (≤7 mg/kg) to anesthetize airways. Biopsies were taken at bifurcations of segmental airways using disposable alligator forceps (Olympus FB-211D-A, Olympus America Inc.).

Immunohistochemistry of lung tissue. Lung tissue samples were fixed in 10% formalin for 2 hours at room temperature prior to paraffin embedding. Any endogenous peroxidase was blocked with 3% H_2O_2 in methanol, and the sections were stained for NLRP3 (1:100, Adipogen) or IL-18 (1:50, Millipore). The sections were incubated for 10 minutes in anti-mouse biotin (M.O.M. kit, catalog BMK-2202, Vector Laboratory) and then incubated for 30 minutes in avidin-biotin-peroxidase complex (Elite ABC kit, Vector Laboratory). Diaminobenzidine (DAB Reagent Set, KPL Laboratory) was used as a chromogen. Counterstaining was performed using hematoxylin. Intensity of staining of airway epithelium was determined using image acquisition and analysis software (ImageJ, NIH) and presented as percentage difference compared with healthy controls. All images used the same imaging settings. The quantity of positive staining in the epithelial layer only was determined by analysis of 3–6 fields of view per slide at ×40. Images were taken at ×40.

Statistics. Data are shown as mean ± SEM. Analysis of experiments was conducted using 2-way ANOVA or 1-way ANOVA, and post-hoc comparisons were tested using Tukey correction. For HAEC experiments and lung section analysis, Student's 2-tailed *t* test was utilized to determine differences. The GraphPad Prism statistical software program was used for the analyses. $P < 0.05$ was regarded as statistically significant.

Study approval. The study was approved by the Vanderbilt University Committee for the Protection of Human Subjects. All animal care and housing requirements of the NIH Committee on Care and Use of Laboratory Animals were followed. All protocols were reviewed and approved by the University of Iowa Animal Care and Use Committee.

Author contributions

IMG, MEA, OMK, OAJ, FSS, and SCS designed experiments, and MEA, IMG, RD, FSS, and SCS analyzed data and wrote the paper. Human lung sections were provided by RD. Data were generated by SCS, OMK, OAJ, CJW, and JDP.

Acknowledgments

This work was supported by a University of Iowa Carver College of Medicine Innovative Science grant, NIH grant R01 HL108932 (to IMG), NIH grants K23 HL080030 and M01 RR-00095 (to RD), and NIH grant R56 AI118719 (to FSS). We are indebted to Chantal Allamargot (Central Microscopy Research Facilities, University of Iowa) for expert technical support and to Shawn Roach and Kristina W. Thiel for assistance in the preparation of the manuscript.

Address correspondence to: Isabella Grumbach, Department of Internal Medicine, Carver College of Medicine, University of Iowa, 4336 PBDB, 169 Newton Road, Iowa City, Iowa 52242, USA. Phone: 319.384.4610; E-mail: isabella-grumbach@uiowa.edu.

1. Barnett SB, Nurmagambetov TA. Costs of asthma in the United States: 2002-2007. *J Allergy Clin Immunol*. 2011;127(1):145–152.
2. Barnes PJ. New therapies for asthma: is there any progress? *Trends Pharmacol Sci*. 2010;31(7):335–343.
3. Olin JT, Wechsler ME. Asthma: pathogenesis and novel drugs for treatment. *BMJ*. 2014;349:g5517.
4. Henricks PA, Nijkamp FP. Reactive oxygen species as mediators in asthma. *Pulm Pharmacol Ther*. 2001;14(6):409–420.
5. Sahiner UM, Birben E, Erzurum S, Sackesen C, Kalayci O. Oxidative stress in asthma. *World Allergy Organ J*. 2011;4(10):151–158.
6. Reddy PH. Mitochondrial Dysfunction and Oxidative Stress in Asthma: Implications for Mitochondria-Targeted Antioxidant Therapeutics. *Pharmaceuticals (Basel)*. 2011;4(3):429–456.
7. Agrawal A, Mabalirajan U. Rejuvenating cellular respiration for optimizing respiratory function: targeting mitochondria. *Am J Physiol Lung Cell Mol Physiol*. 2016;310(2):L103–L113.
8. Sanders PN, et al. CaMKII is essential for the proasthmatic effects of oxidation. *Sci Transl Med*. 2013;5(195):195ra97.
9. Erickson JR, et al. A dynamic pathway for calcium-independent activation of CaMKII by methionine oxidation. *Cell*. 2008;133(3):462–474.
10. Jaffer OA, et al. Mitochondrial-targeted antioxidant therapy decreases TGFbeta mediated collagen production in a murine asthma model. *Am J Respir Cell Mol Biol*. 2015;52(1):106–115.
11. Mabalirajan U, et al. Mitochondrial structural changes and dysfunction are associated with experimental allergic asthma. *J Immunol*. 2008;181(5):3540–3548.
12. Aguilera-Aguirre L, Bacsi A, Saavedra-Molina A, Kurosky A, Sur S, Boldogh I. Mitochondrial dysfunction increases allergic airway inflammation. *J Immunol*. 2009;183(8):5379–5387.
13. Brookes PS, Yoon Y, Robotham JL, Anders MW, Sheu SS. Calcium, ATP, and ROS: a mitochondrial love-hate triangle. *Am J Physiol, Cell Physiol*. 2004;287(4):C817–C833.
14. Cloonan SM, Choi AM. Mitochondria in lung disease. *J Clin Invest*. 2016;126(3):809–820.
15. Phaniendra A, Jestadi DB, Periyasamy L. Free radicals: properties, sources, targets, and their implication in various diseases. *Indian J Clin Biochem*. 2015;30(1):11–26.
16. Kim SR, et al. NLRP3 inflammasome activation by mitochondrial ROS in bronchial epithelial cells is required for allergic inflammation. *Cell Death Dis*. 2014;5:e1498.
17. Xu YD, et al. The early asthmatic response is associated with glycolysis, calcium binding and mitochondria activity as revealed by proteomic analysis in rats. *Respir Res*. 2010;11:107.
18. You Y, Richer EJ, Huang T, Brody SL. Growth and differentiation of mouse tracheal epithelial cells: selection of a proliferative population. *Am J Physiol Lung Cell Mol Physiol*. 2002;283(6):L1315–L1321.
19. Karp PH, et al. An in vitro model of differentiated human airway epithelia. Methods for establishing primary cultures. *Methods Mol Biol*. 2002;188:115–137.
20. Joiner ML, et al. CaMKII determines mitochondrial stress responses in heart. *Nature*. 2012;491(7423):269–273.
21. Chang BH, Mukherji S, Soderling TR. Characterization of a calmodulin kinase II inhibitor protein in brain. *Proc Natl Acad Sci USA*. 1998;95(18):10890–10895.
22. Pan J, et al. Honokiol inhibits lung tumorigenesis through inhibition of mitochondrial function. *Cancer Prev Res (Phila)*. 2014;7(11):1149–1159.
23. Abe Y, Sakairi T, Beeson C, Kopp JB. TGF-β1 stimulates mitochondrial oxidative phosphorylation and generation of reactive oxygen species in cultured mouse podocytes, mediated in part by the mTOR pathway. *Am J Physiol Renal Physiol*. 2013;305(10):F1477–F1490.
24. Watson B, Gauvreau GM. Thymic stromal lymphopoietin: a central regulator of allergic asthma. *Expert Opin Ther Targets*. 2014;18(7):771–785.
25. Pease JE, Williams TJ. Eotaxin and asthma. *Curr Opin Pharmacol*. 2001;1(3):248–253.
26. Wright JG, Christman JW. The role of nuclear factor kappa B in the pathogenesis of pulmonary diseases: implications for therapy. *Am J Respir Med*. 2003;2(3):211–219.
27. Pantano C, et al. Nuclear factor-kappaB activation in airway epithelium induces inflammation and hyperresponsiveness. *Am J Respir Crit Care Med*. 2008;177(9):959–969.

28. Hart LA, Krishnan VL, Adcock IM, Barnes PJ, Chung KF. Activation and localization of transcription factor, nuclear factor-kappaB, in asthma. *Am J Respir Crit Care Med*. 1998;158(5 Pt 1):1585–1592.
29. Yang L, Cohn L, Zhang DH, Homer R, Ray A, Ray P. Essential role of nuclear factor kappaB in the induction of eosinophilia in allergic airway inflammation. *J Exp Med*. 1998;188(9):1739–1750.
30. Li X, Fang P, Mai J, Choi ET, Wang H, Yang XF. Targeting mitochondrial reactive oxygen species as novel therapy for inflammatory diseases and cancers. *J Hematol Oncol*. 2013;6:19.
31. Tully JE, et al. Epithelial NF-κB orchestrates house dust mite-induced airway inflammation, hyperresponsiveness, and fibrotic remodeling. *J Immunol*. 2013;191(12):5811–5821.
32. Wilson RH, Whitehead GS, Nakano H, Free ME, Kolls JK, Cook DN. Allergic sensitization through the airway primes Th17-dependent neutrophilia and airway hyperresponsiveness. *Am J Respir Crit Care Med*. 2009;180(8):720–730.
33. He M, et al. Desert dust induces TLR signaling to trigger Th2-dominant lung allergic inflammation via a MyD88-dependent signaling pathway. *Toxicol Appl Pharmacol*. 2016;296:61–72.
34. Ferreira TP, et al. Potential of PEGylated Toll-like receptor 7 ligands for controlling inflammation and functional changes in mouse models of asthma and silicosis. *Front Immunol*. 2016;7:95.
35. Boaru SG, Borkham-Kamphorst E, Van de Leur E, Lehnen E, Liedtke C, Weiskirchen R. NLRP3 inflammasome expression is driven by NF-κB in cultured hepatocytes. *Biochem Biophys Res Commun*. 2015;458(3):700–706.
36. Cogswell JP, et al. NF-kappa B regulates IL-1 beta transcription through a consensus NF-kappa B binding site and a nonconsensus CRE-like site. *J Immunol*. 1994;153(2):712–723.
37. Possa SS, Leick EA, Prado CM, Martins MA, Tibério IF. Eosinophilic inflammation in allergic asthma. *Front Pharmacol*. 2013;4:46.
38. Zhou LF, Zhang MS, Hu AH, Zhu Z, Yin KS. Selective blockade of NF-kappaB by novel mutated IkappaBalpha suppresses CD3/CD28-induced activation of memory CD4+ T cells in asthma. *Allergy*. 2008;63(5):509–517.
39. Sonar SS, et al. Clara cells drive eosinophil accumulation in allergic asthma. *Eur Respir J*. 2012;39(2):429–438.
40. Lambrecht BN, Hammad H. The airway epithelium in asthma. *Nat Med*. 2012;18(5):684–692.
41. Conroy DM, Williams TJ. Eotaxin and the attraction of eosinophils to the asthmatic lung. *Respir Res*. 2001;2(3):150–156.
42. Pope SM, et al. Identification of a cooperative mechanism involving interleukin-13 and eotaxin-2 in experimental allergic lung inflammation. *J Biol Chem*. 2005;280(14):13952–13961.
43. Steinke JW, Borish L. Th2 cytokines and asthma. Interleukin-4: its role in the pathogenesis of asthma, and targeting it for asthma treatment with interleukin-4 receptor antagonists. *Respir Res*. 2001;2(2):66–70.
44. Birrell MA, Eltom S. The role of the NLRP3 inflammasome in the pathogenesis of airway disease. *Pharmacol Ther*. 2011;130(3):364–370.
45. Bruchard M, et al. The receptor NLRP3 is a transcriptional regulator of TH2 differentiation. *Nat Immunol*. 2015;16(8):859–870.
46. Hussain S, et al. Inflammasome activation in airway epithelial cells after multi-walled carbon nanotube exposure mediates a profibrotic response in lung fibroblasts. *Part Fibre Toxicol*. 2014;11:28.
47. Zhou R, Yazdi AS, Menu P, Tschopp J. A role for mitochondria in NLRP3 inflammasome activation. *Nature*. 2011;469(7329):221–225.
48. Heid ME, Keyel PA, Kamga C, Shiva S, Watkins SC, Salter RD. Mitochondrial reactive oxygen species induces NLRP3-dependent lysosomal damage and inflammasome activation. *J Immunol*. 2013;191(10):5230–5238.
49. Bulua AC, et al. Mitochondrial reactive oxygen species promote production of proinflammatory cytokines and are elevated in TNFR1-associated periodic syndrome (TRAPS). *J Exp Med*. 2011;208(3):519–533.
50. Nakahira K, et al. Autophagy proteins regulate innate immune responses by inhibiting the release of mitochondrial DNA mediated by the NALP3 inflammasome. *Nat Immunol*. 2011;12(3):222–230.
51. Li H, Willingham SB, Ting JP, Re F. Cutting edge: inflammasome activation by alum and alum's adjuvant effect are mediated by NLRP3. *J Immunol*. 2008;181(1):17–21.
52. Coll RC, et al. A small-molecule inhibitor of the NLRP3 inflammasome for the treatment of inflammatory diseases. *Nat Med*. 2015;21(3):248–255.
53. Park CS, et al. Increased oxidative stress in the airway and development of allergic inflammation in a mouse model of asthma. *Ann Allergy Asthma Immunol*. 2009;103(3):238–247.
54. Sureshbabu A, Bhandari V. Targeting mitochondrial dysfunction in lung diseases: emphasis on mitophagy. *Front Physiol*. 2013;4:384.
55. Timmins JM, et al. Calcium/calmodulin-dependent protein kinase II links ER stress with Fas and mitochondrial apoptosis pathways. *J Clin Invest*. 2009;119(10):2925–2941.
56. Westenbrink BD, et al. Mitochondrial reprogramming induced by CaMKIIδ mediates hypertrophy decompensation. *Circ Res*. 2015;116(5):e28–e39.
57. Mishra S, Gray CB, Miyamoto S, Bers DM, Brown JH. Location matters: clarifying the concept of nuclear and cytosolic CaMKII subtypes. *Circ Res*. 2011;109(12):1354–1362.
58. Xiang YY, et al. A GABAergic system in airway epithelium is essential for mucus overproduction in asthma. *Nat Med*. 2007;13(7):862–867.
59. Jeulin C, Guadagnini R, Marano F. Oxidant stress stimulates Ca2+-activated chloride channels in the apical activated membrane of cultured nonciliated human nasal epithelial cells. *Am J Physiol Lung Cell Mol Physiol*. 2005;289(4):L636–L646.
60. Alevy YG, et al. IL-13-induced airway mucus production is attenuated by MAPK13 inhibition. *J Clin Invest*. 2012;122(12):4555–4568.
61. Newcomb DC, et al. IL-17A induces signal transducers and activators of transcription-6-independent airway mucous cell metaplasia. *Am J Respir Cell Mol Biol*. 2013;48(6):711–716.
62. Neveu WA, et al. IL-6 is required for airway mucus production induced by inhaled fungal allergens. *J Immunol*. 2009;183(3):1732–1738.
63. Rincon M, Irvin CG. Role of IL-6 in asthma and other inflammatory pulmonary diseases. *Int J Biol Sci*. 2012;8(9):1281–1290.
64. Pantano C, Reynaert NL, van der Vliet A, Janssen-Heininger YM. Redox-sensitive kinases of the nuclear factor-kappaB signaling pathway. *Antioxid Redox Signal*. 2006;8(9-10):1791–1806.
65. Morgan MJ, Liu ZG. Crosstalk of reactive oxygen species and NF-κB signaling. *Cell Res*. 2011;21(1):103–115.
66. Payne CM, et al. Deoxycholate induces mitochondrial oxidative stress and activates NF-kappaB through multiple mechanisms

in HCT-116 colon epithelial cells. *Carcinogenesis*. 2007;28(1):215–222.
67. Kashiwase K, et al. CaMKII activates ASK1 and NF-kappaB to induce cardiomyocyte hypertrophy. *Biochem Biophys Res Commun*. 2005;327(1):136–142.
68. Weinreuter M, et al. CaM Kinase II mediates maladaptive post-infarct remodeling and pro-inflammatory chemoattractant signaling but not acute myocardial ischemia/reperfusion injury. *EMBO Mol Med*. 2014;6(10):1231–1245.
69. Zorov DB, Juhaszova M, Sollott SJ. Mitochondrial reactive oxygen species (ROS) and ROS-induced ROS release. *Physiol Rev*. 2014;94(3):909–950.
70. Han YG, Choi SM, Kim SH, Lee SB. Voltage-controllable wavelength-selective optical switching based on multiply cascaded long-period fiber gratings. *Opt Lett*. 2003;28(21):2034–2036.
71. Turrens JF. Mitochondrial formation of reactive oxygen species. *J Physiol (Lond)*. 2003;552(Pt 2):335–344.
72. Chandel NS, Schumacker PT, Arch RH. Reactive oxygen species are downstream products of TRAF-mediated signal transduction. *J Biol Chem*. 2001;276(46):42728–42736.
73. Roshak AK, Callahan JF, Blake SM. Small-molecule inhibitors of NF-kappaB for the treatment of inflammatory joint disease. *Curr Opin Pharmacol*. 2002;2(3):316–321.
74. Traba J, et al. Fasting and refeeding differentially regulate NLRP3 inflammasome activation in human subjects. *J Clin Invest*. 2015;125(12):4592–4600.
75. Kim HY, et al. Interleukin-17-producing innate lymphoid cells and the NLRP3 inflammasome facilitate obesity-associated airway hyperreactivity. *Nat Med*. 2014;20(1):54–61.
76. Wu J, Yan Z, Schwartz DE, Yu J, Malik AB, Hu G. Activation of NLRP3 inflammasome in alveolar macrophages contributes to mechanical stretch-induced lung inflammation and injury. *J Immunol*. 2013;190(7):3590–3599.
77. Hosseinian N, Cho Y, Lockey RF, Kolliputi N. The role of the NLRP3 inflammasome in pulmonary diseases. *Ther Adv Respir Dis*. 2015;9(4):188–197.
78. Koch KN, et al. Helicobacter urease-induced activation of the TLR2/NLRP3/IL-18 axis protects against asthma. *J Clin Invest*. 2015;125(8):3297–3302.
79. Kim HY, et al. Mitochondrial Ca(2+) uptake is essential for synaptic plasticity in pain. *J Neurosci*. 2011;31(36):12982–12991.
80. Luczak ED, Anderson ME. CaMKII oxidative activation and the pathogenesis of cardiac disease. *J Mol Cell Cardiol*. 2014;73:112–116.
81. Rawlins EL, et al. The role of Scgb1a1+ Clara cells in the long-term maintenance and repair of lung airway, but not alveolar, epithelium. *Cell Stem Cell*. 2009;4(6):525–534.
82. Singh MV, et al. Ca2+/calmodulin-dependent kinase II triggers cell membrane injury by inducing complement factor B gene expression in the mouse heart. *J Clin Invest*. 2009;119(4):986–996.
83. Dikalova A, et al. Nox1 overexpression potentiates angiotensin II-induced hypertension and vascular smooth muscle hypertrophy in transgenic mice. *Circulation*. 2005;112(17):2668–2676.
84. He C, Murthy S, McCormick ML, Spitz DR, Ryan AJ, Carter AB. Mitochondrial Cu,Zn-superoxide dismutase mediates pulmonary fibrosis by augmenting H2O2 generation. *J Biol Chem*. 2011;286(17):15597–15607.
85. National Asthma Education Prevention Program. Expert Panel Report 3 (EPR-3): Guidelines for the Diagnosis and Management of Asthma-Summary Report 2007. *J Allergy Clin Immunol*. 2007;120(5 Suppl):S94–138.
86. Bernstein IL, et al. Allergy diagnostic testing: an updated practice parameter. *Ann Allergy Asthma Immunol*. 2008;100(3 Suppl 3):S1–148.
87. Crapo RO, et al. Guidelines for methacholine and exercise challenge testing-1999. This official statement of the American Thoracic Society was adopted by the ATS Board of Directors, July 1999. *Am J Respir Crit Care Med*. 2000;161(1):309–329.
88. Cockcroft DW, et al. The links between allergen skin test sensitivity, airway responsiveness and airway response to allergen. *Allergy*. 2005;60(1):56–59.